Use of probability distribution functions for discriminating between cloud and aerosol in lidar backscatter data

Zhaoyan Liu,[1] Mark A. Vaughan,[2] David M. Winker,[3] Chris A. Hostetler,[3] Lamont R. Poole,[3] Dennis Hlavka,[4] William Hart,[4] and Matthew McGill[5]

Received 3 March 2004; revised 19 May 2004; accepted 3 June 2004; published 7 August 2004.

[1] In this paper, we describe the algorithm that will be used during the upcoming Cloud-Aerosol Lidar and Infrared Pathfinder Satellite Observations (CALIPSO) mission for discriminating between clouds and aerosols detected in two-wavelength backscatter lidar profiles. We first analyze single-test and multiple-test classification approaches based on one-dimensional (1-D) and multidimensional probability distribution functions (PDFs) in the context of a two-class feature identification scheme. From these studies we derive an operational algorithm. This algorithm is a 3-D approach utilizing the layer mean attenuated backscatter at 532 nm, the layer-integrated 1064-nm to 532-nm volume color ratio, and the midlayer altitude. A data set acquired by the Cloud Physics Lidar (CPL) is used to test the algorithm. Comparisons are conducted between the 3-D CALIPSO algorithm results and those derived from an existing 2-D algorithm. The results obtained show generally good agreement between the two methods. However, of a total of 228,264 layers analyzed, ~5.7% are classified as different types by the two algorithms. This disparity is shown to be due largely to the misclassification of optically thin clouds as aerosols by the 2-D algorithm. The use of 3-D PDFs in the CALIPSO algorithm is found to significantly reduce this type of error because the separation between cloud and aerosol clusters is more complete in this 3-D space. Dust presents a special case. Because the intrinsic scattering properties of dust layers can be very similar to those of clouds, additional algorithm testing was performed using an optically dense layer of Saharan dust measured during the Lidar In-space Technology Experiment (LITE). In general, the method is shown to distinguish reliably between dust layers and clouds. The relatively few erroneous classifications that occurred most often in the analysis of the LITE data occurred in those regions of the Saharan dust layer where the optical thickness was the highest. *INDEX TERMS:* 0933 Exploration Geophysics: Remote sensing; 0910 Exploration Geophysics: Data processing; 1704 History of Geophysics: Atmospheric sciences; *KEYWORDS:* scene classification, cloud and aerosol discrimination, space lidar

Citation: Liu, Z., M. A. Vaughan, D. M. Winker, C. A. Hostetler, L. R. Poole, D. Hlavka, W. Hart, and M. McGill (2004), Use of probability distribution functions for discriminating between cloud and aerosol in lidar backscatter data, *J. Geophys. Res.*, *109*, D15202, doi:10.1029/2004JD004732.

1. Introduction

[2] The excellent spatial resolution provided by backscatter lidar makes it a powerful remote sensing tool for measuring the vertical distribution of clouds and aerosols in Earth's atmosphere. When flown in space, backscatter lidars can provide measurements of clouds and aerosols on a global scale. This unique ability has been demonstrated by NASA's Lidar In-space Technology Experiment (LITE) [*Winker et al.*, 1996]. However, the quantitative retrieval of cloud and aerosol optical properties, including backscatter and extinction profiles and layer optical depths, requires knowledge of the extinction-to-backscatter ratio (or the "lidar ratio"). Given a sufficiently accurate measurement of the layer two-way transmittance [e.g., *Young*, 1995; *Liu et al.*, 2000], or (alternately) simultaneous two-wavelength, high signal-to-noise ratio (SNR) measurements for which the backscatter profiles satisfy some additional similarity requirements [e.g., *Sasano and Browell*, 1989; *Liu et al.*, 2000; *Vaughan*, 2003], the lidar ratio can be retrieved from the lidar observation alone. However, for space-based lidar measurements these conditions are only occasionally satisfied, and therefore the specific values of lidar ratio that are applied in the data processing must be selected according to an informed estimate of the layer type and/or composition. In this latter case, accurate selection of lidar ratio relies on a

[1]Center for Atmospheric Sciences, Hampton University, Hampton, Virginia, USA.
[2]Science Applications International Corporation, Hampton, Virginia, USA.
[3]NASA Langley Research Center, Hampton, Virginia, USA.
[4]Science Systems and Applications, Inc., Greenbelt, Maryland, USA.
[5]NASA Goddard Space Flight Center, Greenbelt, Maryland, USA.

Copyright 2004 by the American Geophysical Union.
0148-0227/04/2004JD004732$09.00

layer classification scheme that determines layer type on the basis of inferential tests applied to the directly measurable optical and physical properties of the layer. These properties include attenuated backscatter coefficients, attenuated total color ratios, volume depolarization ratios, layer top, base, and/or center height, geophysical location, season, etc.

[3] The work reported in this paper develops a fully automated scene classification algorithm for discriminating between clouds and aerosols in lidar data to be acquired by Cloud-Aerosol Lidar and Infrared Pathfinder Satellite Observations (CALIPSO). The CALIPSO mission is being developed jointly by NASA and the French space agency, Centre National d'Etudes Spatiales [*Winker et al.*, 2003]. Its payload consists of a polarization-sensitive two-wavelength lidar, an imaging infrared radiometer, and a wide field camera. Together, this suite of instruments will provide a unique set of measurements to improve our understanding of the role of clouds and aerosols in the Earth's climate system. After launch in early 2005 the CALIPSO satellite will conduct on-orbit observations continuously for 3 years. The tremendous data volume acquired during this time necessitates the use of a fully automated data analysis system. To this end, a collection of intelligent algorithms for automated CALIPSO lidar data processing is being developed [*Liu et al.*, 2002b; *Hu et al.*, 2001; *Omar et al.*, 2002; *Vaughan et al.*, 2002; *Reagan et al.*, 2002]. Of fundamental importance in this processing is the accurate discrimination between clouds and aerosols in the backscatter data. Cloud-aerosol discrimination is important not only in the selection of appropriate lidar ratios for extinction retrievals but also, more fundamentally, so that aerosol retrievals are not contaminated by clouds. Cloud contamination is one of the primary uncertainties in current aerosol climatologies derived from passive satellite observations. The range-resolved data acquired by satellite lidar significantly improve our ability to discriminate cloud from aerosol, and should therefore greatly enhance our ability to make reliable aerosol measurements in broken-cloud environments.

[4] In this paper, we investigate classification techniques for distinguishing between two separate classes on the basis of probability distribution functions (PDFs) and propose a specific variant for use during the CALIPSO mission. We first introduce different classification approaches based on a single test or on multiple tests that use a confidence function (*f*-function) constructed from one-dimensional and multidimensional (1-D or multiple-D) probability distribution functions to distinguish between two classes. We then develop an operational algorithm for cloud-aerosol discrimination that takes full advantage of the measurements made by the polarization-sensitive, two-wavelength lidar flown aboard the CALIPSO satellite. Extensive tests of algorithm performance were conducted using approximately 49 hours of down-looking lidar data obtained by the Cloud Physics Lidar (CPL) [*McGill et al.*, 2002] during the 2003 Observing System Research and Predictability Experiment–Pacific THORPEX Observing System Test (THORPEX-PTOST) campaign (M. A. Shapiro and A. J. Thorpe, Program overview, 2002, available at http://www-angler.larc.nasa.gov/thorpex/index.html). Additional algorithm tests focused on the correct identification of dust layers as aerosols. These tests used measurements of an optically and geometrically thick layer of Saharan dust acquired during orbit 83 of the LITE mission [*Winker et al.*, 1996]. Test results for both cases are presented, and for the THORPEX data the CALIPSO classifications are compared to those obtained by a 2-D algorithm originally developed for the Geoscience Laser Altimeter System (GLAS) data processing.

2. Classification Approaches

2.1. Algorithm Overview

[5] *Wang and Sassen* [2001] have recently developed a rule-based algorithm for cloud type classification of ground-based observations from multiple remote sensors. For successful cloud typing, clouds must first be distinguished from aerosol layers. In this procedure the discrimination between clouds and aerosols is achieved by comparing the observed ratio of peak-to-base signals, T, in a layer with some preselected value. The feature is classified as an aerosol when T is smaller than this value, and as a cloud otherwise. In effect, the Wang and Sassen approach to cloud-aerosol discrimination can be seen as a thresholding technique, with the preselected T ratio serving as a threshold value separating clouds and aerosols. The specification of the threshold value becomes more critical at higher altitudes (>5 km), because of the increased occurrence of subvisual and thin cirrus having T values close to those characteristic of aerosols. In addition, optimal performance of the Wang and Sassen algorithm requires high-SNR samples acquired by averaging over a time window of 1 hour (i.e., sixty 1-min-averaged profiles). This last requirement raises some practical concerns about the application of their technique to space-based lidar measurements. Mass and power constraints for orbiting systems typically dictate a very low per-pulse SNR. This limitation is exacerbated by the very rapid movement of the sensor across the Earth's surface, which restricts the observation time for any single feature and consequently precludes the use of extensive temporal averaging to improve the SNR.

[6] A second variant of the threshold algorithm has been developed for use by GLAS [*Palm et al.*, 2002], and a prototype of this algorithm has been implemented for testing in the CPL analysis software. The GLAS prototype algorithm is applied to the attenuated volume backscatter coefficients $\beta'(r)$ [*Platt et al.*, 1998], i.e., to the calibrated, range-corrected lidar signals within each layer. The discriminator applied when using this technique is the product, P, of the layer's maximum attenuated backscatter, $\beta'_{\max}$, and maximum vertical gradient magnitude within the layer, $|\Delta\beta'/\Delta z|_{\max}$. Computed P values are then compared to a predetermined, altitude-dependent array of threshold values. Layers with values of P in excess of the threshold are interpreted as cloud; those with P values uniformly less than the threshold are classified as aerosols. As with the *Wang and Sassen* [2001] algorithm, the selection of threshold values is crucial. The GLAS threshold values for each altitude bin are set at the point where the probability of correct cloud designation is the highest when balanced against the probability of false aerosol designation. The probabilities used are derived from statistical studies of existing ground-based and airborne databases. The GLAS algorithm is therefore equivalent to a 2-D (in p-z space) algorithm. Difficulties in applying this approach to space

lidar may arise from the gradient computation of $|\Delta\beta'/\Delta z|_{max}$. Because the gradient calculation is highly sensitive to noise, and because the SNR for space-based lidars is generally poor when compared to ground-based or airborne system, P values computed from space lidar data are likely to be highly uncertain.

[7] Unlike the techniques described previously, the cloud-aerosol discrimination technique devised for the CALIPSO lidar measurements is a PDF-based approach. Classifications derived using these techniques are based on statistical differences exhibited by the various optical and physical properties of clouds and aerosols [*Liu et al.*, 2002b]. A confidence function constructed from 1-D or multiple-D PDFs of feature attributes is introduced to serve as the discriminator between two classes. Along with the classification decision, PDF-based approaches can also assign a confidence level to each decision. In addition, because the inference engine performing the classifications is designed to be independent of the PDF database, new knowledge obtained via lidar observation or from other data sources can be used to update the PDF database without requiring modifications of the engine. In the following sections we introduce the general concepts inherent in the PDF-based classification approaches and describe some specific implementations.

2.2. Single-Test Classification

[8] The confidence function on which the PDF-based approaches rely is given by [*Liu et al.*, 2002b]

$$f(X) = \frac{n_2(X) - n_1(X)}{n_2(X) + n_1(X)} = \frac{P_2(X) - P_1(X)N_1/N_2}{P_2(X) + P_1(X)N_1/N_2} = \frac{P_2(X) - P_1(X)K_s}{P_2(X) + P_1(X)K_s}. \quad (1)$$

In this expression, X is the value of a given test attribute used to classify the feature. For the CALIPSO cloud-aerosol discrimination task, X can be the attenuated backscatter, attenuated volume color ratio, depolarization ratio, etc. The $n_i(X)$ and N_i are the number of occurrences of class i having attribute X and the total number of events for the ith class, respectively. $P(X)$ is the PDF of X. $K_s = N_1/N_2$ is therefore a scale factor that quantifies the relative occurrence frequency of the two classes. Subscripts 1 and 2 refer to classes 1 and 2, i.e., to aerosol and cloud, respectively, when the technique is applied to the cloud-aerosol discrimination problem. Alternately, subscripts 1 and 2 could refer to water and ice should the technique be applied to the cloud phase discrimination problem. We note that $n_1/(n_1 + n_2)$ and $n_2/(n_1 + n_2)$ are the occurrence probabilities of classes 1 and 2, respectively, and therefore f is the differential occurrence probability. As shown conceptually in Figure 1, the value returned by the confidence function is bounded on $[-1, 1]$.

[9] On the basis of the return value of the f-function we derive both a classification and a measure of the confidence we ascribe to that classification. The sign of the f-function determines the class assignment; as in Figure 1b, negative values indicate class 1, and positive values indicate class 2. The magnitude of f (between 0 and 1) assigns a confidence to the classification. A value of zero indicates that no classification can be made. All lower confidence classifications arise from the overlap region of the two PDFs, shown between A and A′ in Figure 1a.

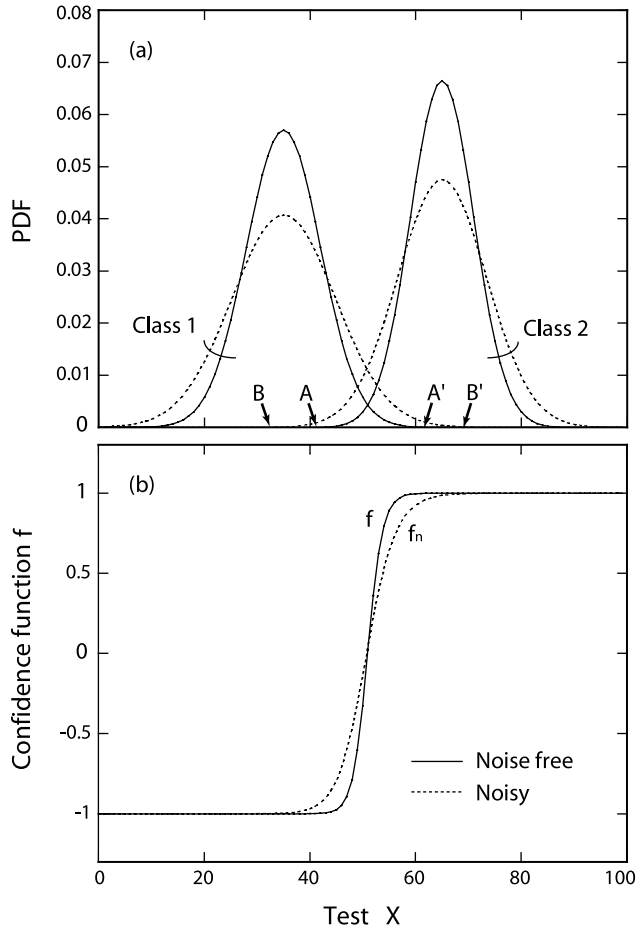

Figure 1. Conceptual (a) PDFs and (b) confidence functions, showing that the effect of noise is to widen the PDFs and thereby increase the PDF overlap and region of ambiguity where the magnitude of confidence function is smaller than 1.

[10] Noise and systematic errors in observation data can further reduce the confidence of decision. As shown in the following discussion, noise can broaden the measured PDFs of a test attribute. The noise-affected confidence function $f_n(X)$ can be introduced using the noise-affected PDFs $P_{i,n}$ (i = 1 or 2 represents classes 1 or 2):

$$f_n(X) = \frac{P_{2,n}(X) - P_{1,n}(X)K_s}{P_{2,n}(X) + P_{1,n}(X)K_s}, \quad (2)$$

$$P_{i,n}(X) = \int_0^\infty P_i(\tilde{X}) p_{noise}(X, \tilde{X}) d\tilde{X}. \quad (3)$$

Here $p_{noise}(X, \tilde{X})$ is the distribution of variations in test X centered at $\tilde{X}$ induced by the noise, i.e., the probability that a true value of $\tilde{X}$ will be represented as a value of X due solely to noise contamination. To show the noise effect, the noise-affected PDFs computed using equation (3) are also presented in Figure 1a (dashed curves). Gaussian-distributed noise has been assumed with a width 0.4 times that of the noise-free PDFs. The noise-affected PDFs are broadened significantly,

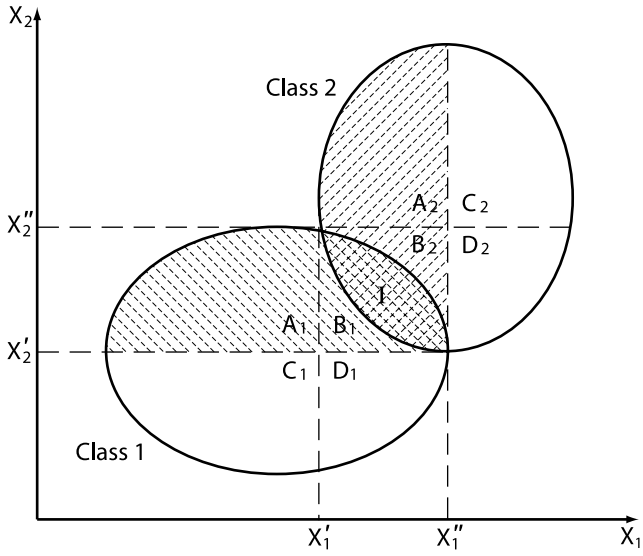

Figure 2. Conceptual two-dimensional PDFs.

and the PDF overlap region is increased. As a result, the low-confidence region in f (the region bounded by B and B′ in Figure 1a) is similarly increased.

2.3. Multiple-Test Classification

[11] As described in section 2.2, there exists an ambiguous, low-confidence region in the f-function where the class 1 and class 2 PDF curves overlap (Figure 1). If the measured value of an observed feature falls within this region, the feature cannot be identified authoritatively; that is, there is a possibility that an erroneous classification is made. However, given a feature described by multiple attributes, should the value of a single test fall within the low-confidence region, it may still be that tests applied to some other attribute will generate a result in the high-confidence region, hence yielding a highly confident classification. The ambiguous classification problem can therefore be improved by conducting multiple tests. We illustrate the situation further by considering the two-test example conceptually illustrated in Figure 2. The boundaries of the class 1 and class 2 clusters are shown by solid curves. We note that in the 2-D example, the 1-D cluster distribution for one test is an integral of the 2-D distribution over another test. The ambiguous region is therefore the area bounded by the line X_1' and X_1'' for test X_1 and by the line X_2' and X_2'' for test X_2; i.e., the region consisting of the areas A_1, B_1, I, B_2, and D_2 for X_2 and A_2, B_2, I, B_1, and D_1 for X_1. The class membership for features in areas D_1 or A_2 cannot be decided unambiguously by test X_1 only. They can, however, be identified by test X_2 since these features are not in the ambiguous region of X_2. It is obvious that features in the areas C_1 and C_2 can be classified unambiguously by either X_1 or X_2, because these features are not in the ambiguous regions of X_1 or X_2. Note that features in the areas B_1, I, and B_2 cannot be classified unambiguously by either test.

[12] A straightforward formulation of a multitest approach is

$$f = f_{\max},$$
$$|f_{\max}| = \max\{|f(X_{1,n})|, |f(X_{2,n})|, \cdots, |f(X_{m,n})|\}, \tag{4}$$

and m is the number of available tests. This approach searches first the test that has the maximal value of the f-function. The classification can then be made on the basis of this max-value test in the same way as the single-test approach described above: The sign of the test determines the feature classification, and the magnitude of the test assigns a confidence value to the classification.

[13] However, using the max-value approach, we still cannot derive an unambiguous classification for the areas B_1, I, and B_2 shown in the example given in Figure 2. Therefore, to further improve our classification efficiency, we introduce a multidimensional confidence function,

$$f_n(X_1, X_2, \cdots, X_m) = \frac{P_{2,n}(X_1, X_2, \cdots, X_m) - P_{1,n}(X_1, X_2, \cdots, X_m)K_s}{P_{2,n}(X_1, X_2, \cdots, X_m) + P_{1,n}(X_1, X_2, \cdots, X_m)K_s}. \tag{5}$$

$P_{i,n}(X_1, X_2, \cdots, X_m)$ is the noise-affected PDF for the ith class and can be derived by

$$P_{i,n}(X_1, X_2, \cdots, X_m) = \int\int\cdots\int P_i(\tilde{X}_1, \tilde{X}_2, \cdots, \tilde{X}_m) p_{\text{noise}}(X_1, \tilde{X}_1) p_{\text{noise}}(X_2, \tilde{X}_2) \cdots p_{\text{noise}}(X_m, \tilde{X}_m)\, d\tilde{X}_1\, d\tilde{X}_2 \cdots d\tilde{X}_m, \tag{6}$$

where $P_i(X_1, X_2, \cdots, X_m)$ is the noise-free multidimensional PDF as a function of test attributes (X_1, X_2, $\cdots$, X_m). The features in areas B_1 and B_2 that are not definitely recognizable by the max-value approach become clearly distinguishable by the multiple-D approach.

[14] In the example given in Figure 2, area I remains an ambiguous region; even the 2-D confidence function approach will not produce an unambiguous classification for features falling in this region. However, by increasing the number of tests (and simultaneously increasing the dimension of the confidence function) it may be possible to further reduce the ambiguous region. From a statistical point of view the separation of different class clusters in higher-dimensional space is generally more complete than in lower dimensional space. Increasing the number of dimensions should decrease the region of complete overlap between the two PDFs, thereby reducing the fraction of ambiguous classifications that are retrieved. This can be seen clearly in the example in Figure 2, where the 2-D cluster distributions have smaller overlap than the 1-D distributions of any test.

3. A Cloud and Aerosol Discrimination Algorithm

3.1. Detail of Algorithm

[15] The lidar cloud-aerosol discrimination is performed on the basis of statistical differences between the spatial and optical properties of clouds and aerosols. Figure 3 presents an example of the particulate backscatter coefficients at 532 nm, β_{532}, and the backscatter color ratio, $\chi = \beta_{1064}/\beta_{532}$, for different types of clouds and aerosols that are defined by the Optical Properties of Aerosols and Clouds (OPAC) software package [*Hess et al.*, 1998a, 1998b]. In general, as seen in the plot, clouds have larger

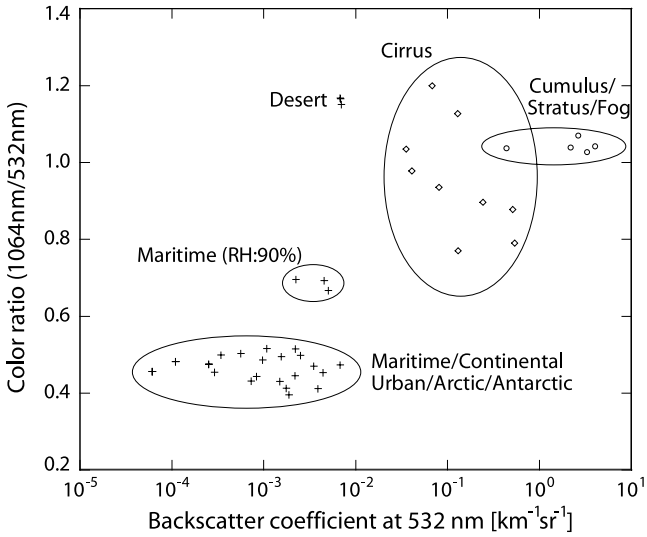

Figure 3. The 1064-nm to 532-nm color ratio versus backscatter coefficient at 532 nm computed with the OPAC software for different types of aerosols and clouds.

backscatter coefficients and higher color ratios around 1. Aerosols have smaller backscatter coefficients and lower color ratios. As borne out by field observations [e.g., *Sugimoto et al.*, 2002], the exceptions to this general rule are desert aerosols and maritime aerosols under high-relative-humidity conditions, both of which exhibit relatively large color ratios. The separation of the cloud and aerosol clusters in the OPAC results clearly indicates the feasibility of using backscatter coefficients and backscatter color ratios to distinguish aerosols from clouds. CALIPSO is designed to make all of the necessary measurements. The CALIPSO lidar is a polarization-sensitive, dual-wavelength system that provides range-resolved measurements of 532-nm and 1064-nm attenuated volume backscatter coefficients. The spectral dependence of the signals from unclassified features can be investigated using the attenuated volume color ratios, which are obtained by dividing the attenuated volume backscatter coefficients at 1064 nm by the identical quantities measured at 532 nm. In addition, because the 532-nm channel is equipped with polarization-sensitive optics, volume depolarization ratios can be derived by taking the ratios of the perpendicular and parallel components of the 532-nm backscatter signal. These optical properties are augmented by layer top and base heights determined by analysis of the profiles of attenuated backscatter coefficients [*Vaughan et al.*, 2002]. This precise spatial information provides an additional constraint that can be used in the scene classification task.

[16] The operational algorithm developed for CALIPSO uses a 3-D approach. Test attributes are the layer-averaged attenuated backscatter β' at 532 nm, the layer-integrated attenuated volume color ratio χ', and the layer center altitude z. The layer-integrated volume color ratio is the ratio formed by dividing the layer-integrated attenuated backscatter at 1064 nm by the layer-integrated attenuated backscatter at 532 nm. The limits of the integration are from layer top to layer base. The layer center altitude is the average of the detected layer top and base altitudes. Including height information with the layer optical properties should increase the effectiveness of any cloud-aerosol separation scheme. This is because the optically thinner clouds that contribute most to the overlap of PDF with aerosols generally appear in higher altitudes, whereas aerosols concentrate mostly in the planetary boundary layer (PBL).

[17] On the basis of modeling studies using OPAC and various analyses of the LITE measurements, it is expected that cloud and aerosol clusters are well resolved in β', χ', and z space. Figure 4 presents a flowchart of the algorithm. The algorithm first loads noise-free PDF files from an existing PDF database that has been compiled on the basis of previous measurements. For each feature, layer products β', χ', and z are read in as input along with estimated uncertainties $\Delta\beta'$ and $\Delta\chi'$. Noise-broadened PDFs are then computed using equation (6). The generation of the necessary noise distributions is described in detail in section 3.2.

3.2. Approximation of the Noise Distribution

[18] To compute the noise-broadened PDFs that allow us to include the effects of measurement noise on the confidence function values obtained using equation (6), distributions of the variations in the test attributes β' and χ' due to noise must first be derived or estimated. The CALIPSO 532-nm and 1064-nm receiver channels use photomultiplier tubes (PMTs) and an avalanche photodiode (APD), respectively, all operated in analog detection mode. PMT signal amplification is a multiply stochastic Neyman type-A process [*Liu and Sugimoto*, 2002]. The multiplication distribution for a uniform gain APD can be analytically described [*McIntyre*, 1972]. However, a Gaussian distribution is a

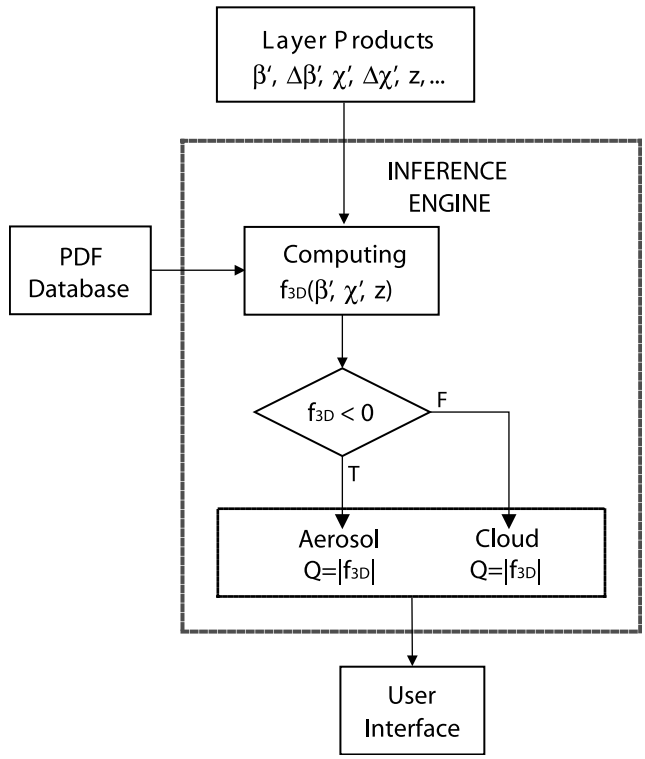

Figure 4. Flowchart of an operational algorithm for the CALIPSO lidar cloud and aerosol classification.

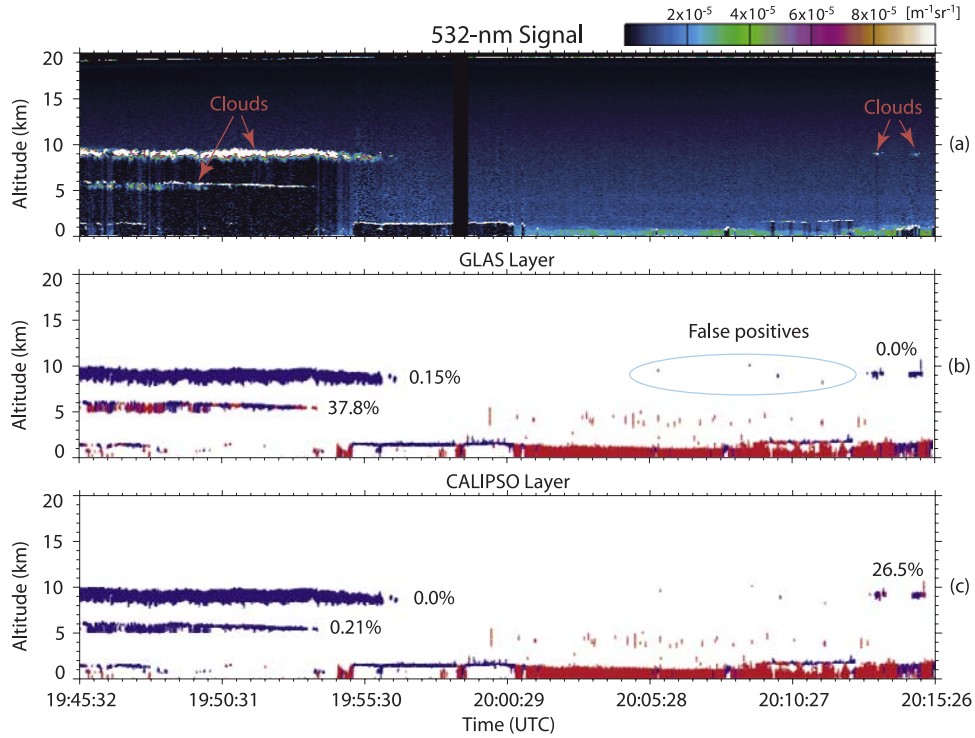

Figure 5. (a) Attenuated backscatter at 532 nm. Feature layer mask classified by (b) the GLAS algorithm and (c) the CALIPSO algorithm.

good approximation for the multiplication process for both PMTs and APDs when the average number of received photoelectrons is larger than ~100. For photon-counting mode the output counts of PMT or APD are distributed in the same way as the input photons. Again, the approximation of Gaussian distribution can be made for larger photoelectron numbers. Our algorithm therefore assumes Gaussian distributions for the noise-induced variations in β' at both 532 nm and 1064 nm. If we designate B and X as the measured values of some underlying true values β' and χ', then the probability that the true value of $\tilde{\beta}'$ is actually measured as B is given by

$$p_{\text{noise}}\left(\mathsf{B},\tilde{\beta}'\right)=\frac{1}{\sqrt{2}\pi\,\sigma_{\tilde{\beta}'}}\exp\left[-\frac{\left(\mathsf{B}-\tilde{\beta}'\right)^2}{2\sigma^2_{\tilde{\beta}'}}\right], \tag{7}$$

where $\sigma_{\tilde{\beta}'}$ is the estimated uncertainty in $\tilde{\beta}'$ due to noise.

[19] The noise distribution for χ' can then be derived from the Gaussian noise distributions of β' at 532-nm and 1064-nm wavelengths:

$$\begin{aligned}p_{\text{noise}}(\chi',\mathsf{X})&=\int_0^\infty p_{\text{noise}}\left(\beta'_{532},\mathsf{B}_{532}\right)p_{\text{noise}}\left(\chi'\beta'_{532},\mathsf{B}_{1064}\right)\beta'^2_{532}\,d\beta'_{532}\\&=\frac{1}{2\pi\sigma_{\mathsf{B}_{532}}\sigma_{\mathsf{B}_{1064}}}\int_0^\infty\exp\left[-\frac{\left(\beta'_{532}-\mathsf{B}_{532}\right)^2}{2\sigma^2_{\mathsf{B}_{532}}}\right.\\&\left.-\frac{\left(\chi'\beta'_{532}-\mathsf{B}_{1064}\right)^2}{2\sigma^2_{\mathsf{B}_{1064}}}\right]\beta'^2_{532}\,d\beta'_{532}.\end{aligned} \tag{8}$$

Here $\sigma_{\mathsf{B}_{532}}$ and $\sigma_{\mathsf{B}_{1064}}$ are the uncertainties estimated for B_{532} and B_{1064}, respectively, and $\mathsf{X}=\mathsf{B}_{1064}/\mathsf{B}_{532}$. The algorithm also assumes that the noise distribution of χ' is the same as that at X over the entire integral region.

4. Algorithm Tests and Discussions

4.1. Using CPL THORPEX-PTOST Data

[20] The Cloud Physics Lidar is a three-wavelength polarization-sensitive airborne lidar system [*McGill et al.*, 2002] that detects the perpendicular and parallel components of the backscatter profile at 1064 nm and total backscatter profiles at 532 nm and 355 nm. Included among the comprehensive suite of CPL postflight data products are feature boundaries, layer type (i.e., cloud or aerosol), and range-resolved extinction and backscatter coefficients. The feature types were classified by the GLAS prototype layer discrimination algorithm. The CPL data sets are thus an ideal data source for CALIPSO algorithm tests, as direct, straightforward comparisons can be made between the CALIPSO test results and the CPL data products. A data set acquired during the 2003 THORPEX-PTOST campaign conducted in Honolulu, Hawaii, from 18 February to 14 March 2003 was used to test the performance of the cloud-aerosol discrimination algorithm. During THORPEX-PTOST the CPL acquired backscatter data on nine scheduled ER-2 flights. The CALIPSO algorithm test set consists of all of the data acquired during these flights. In addition, all data acquired on the ER-2 transit flight from California to Hawaii are also used. In total, the test set consists of approximately 49 hours of CPL measurements.

[21] Figure 5a presents an example of 532-nm attenuated backscatter signals acquired by CPL. The data shown were acquired between 1945:32 and 2015:26 UTC on 19 February 2003. Four high-cloud layers above 5 km are observed.

PBL aerosols as well as some low broken clouds are also seen. An optically thin aerosol layer exists above the PBL and below 5 km. Layer boundaries have been determined by a threshold-based feature finder [*Palm et al.*, 2002] incorporated into the CPL data analysis software. Feature locations, together with the classifications assigned by the GLAS algorithm, are shown in Figure 5b. Colors indicate feature type: Red is aerosol, and blue is cloud. Most layers have been successfully detected, excepting only those optically very thin layers or layers obscured by overlying, optically dense cloud layers. Application of the CPL layer finder to the entire 10-flight data set yields a total of 228,264 features, all of which are used as input to test the CALIPSO cloud-aerosol discrimination algorithm.

[22] For each layer the mean attenuated 532-nm backscatter β'_{532} is derived by averaging the calibrated and range-corrected 532-nm signals over the detected layer upper and lower boundaries. The 1064-nm to 532-nm volume color ratio χ' is obtained from the ratio of the averaged attenuated 1064-nm and 532-nm backscatters, β'_{1064} and β'_{532}. Uncertainty is calculated for each parameter on the basis of error propagation theory [*Bevington and Robinson*, 1992]. Random errors due to noise are dominant when features are optically thin. Only random error is taken into account. Measured layer altitudes are assumed to be accurate.

[23] A PDF database was developed using lidar observations and model data. Consistent with the measurements of *Beyerle et al.* [2001], the mean attenuated volume color ratio for clouds is characterized using a normal distribution. On the basis of the authors' analyses of the LITE data, a normal distribution has also been selected for use with aerosol color ratios. The initial means and standard deviations for the color ratio PDFs were derived from model studies using OPAC. That normal distributions represent appropriate approximations for both cloud and aerosol color ratio distributions can be further verified by inspection of the CPL THORPEX observations (e.g., as shown in Figure 6). A lognormal distribution has been employed to represent the mean attenuated backscatter coefficient for aerosols. Both the LITE data analyses and the lidar measurements acquired at numerous European Aerosol Research Lidar Network (EARLINET) stations show that aerosol backscatter can be well characterized by a lognormal distribution [*Matthias and Bösenberg*, 2002; *Bösenberg et al.*, 2003]. The aerosol backscatter distribution parameters used in this work were derived from the LITE aerosol measurements. For cloud backscatter coefficients we employ a multimodal distribution retrieved from the LITE cloud data. As illustrated in Figure 6, the CPL cloud observations also show a multimodal distribution. In order to automatically accommodate the huge amount of new data that will be collected during the lifetime of CALIPSO, the distribution parameters for both clouds and aerosol can be adjusted iteratively during the classification process. This iterative improvement procedure was employed during the tests with the THORPEX-PTOST data set.

[24] The results produced from the CALIPSO algorithm are quite consistent with the GLAS results: Only 5.7% of a total of 228,264 features have been classified as different types by the GLAS and CALIPSO algorithms. Our case studies showed, however, that the preliminary version of the

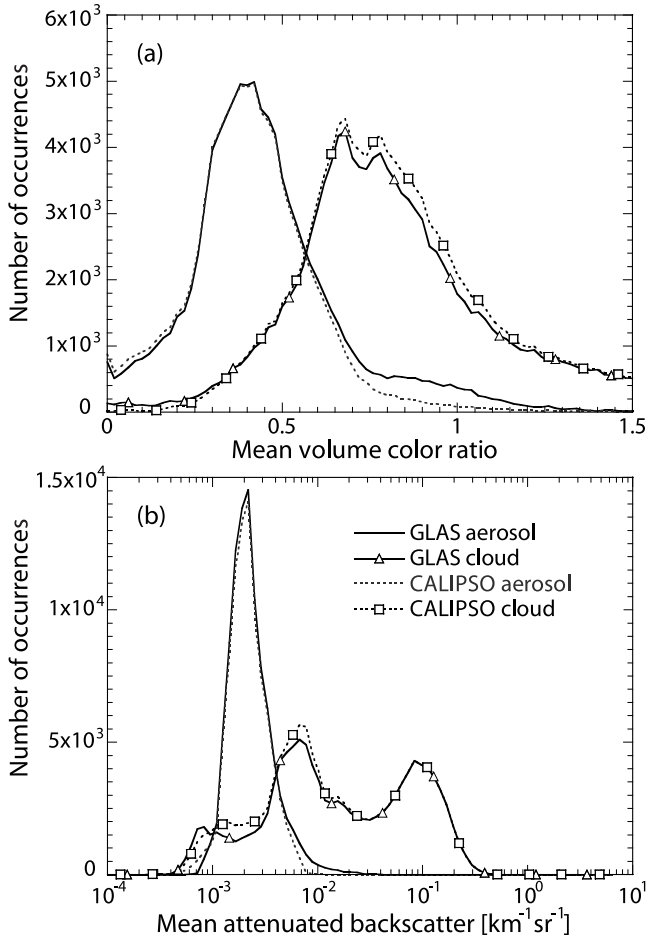

Figure 6. Distributions of (a) volume color ratio and (b) mean attenuated backscatter for all altitudes.

GLAS classification algorithm produced more misclassifications of cloud as illustrated by the example in Figure 5. In this example, ~37.9% of the cloud layer between 5 and 6.5 km from 1945 to 1954 UTC has been incorrectly classified as aerosol by the GLAS algorithm. We note that in the misclassified regions the mean attenuated backscatter has been decreased by the attenuation of the laser beam in the upper cloud layer. On the other hand, however, only 0.21% of this cloud layer has been classified as aerosol by the CALIPSO algorithm, as shown in Figure 5c. The improvement of this layer classification by the CALIPSO algorithm is mainly due to the introduction of the 3-D (β', χ', z) approach. This is because, as will be discussed further below, a better separation of cloud and aerosol clusters can be achieved in this β'-χ'-z space, and the degree of separation of cloud and aerosol clusters is an essential limit on the performance of any scene classification scheme. In addition, the mean attenuated volume color ratio is less sensitive to the attenuation of overlying clouds, because the cloud scattering has weak wavelength dependence in the visible and near-inferred region and, as a result, taking the ratio of the two attenuated backscatter values can cancel the effect of the attenuation of overlaying clouds. The large false rate of this high-cloud layer with the GLAS algorithm might be due in part to the (somewhat arbitrary) threshold value

being not exactly located at the desired balance point that results in an equal false rate for cloud and aerosol. For example, if the selected threshold is larger than the balance value, optically thin clouds can be mistakenly classified as aerosol.

[25] No misclassifications were made by the CALIPSO algorithm in the uppermost cloud layer from 1945 to 1956 UTC. However, the misclassification rate for the two high-cloud layers at 9–10 km on the right-hand side of Figure 5 is quite high (26.5%), because these two layers are optically very thin. Because the GLAS algorithm sets a threshold at 8 km, above which all features are classified as cloud, the GLAS algorithm scores a 100% success rate in these layers. The CALIPSO algorithm includes a similar cutoff threshold, but set at a much higher altitude. The current implementation of the CALIPSO method has the potential to discriminate aerosols up to a maximum altitude of 14 km.

[26] The CPL feature-finding algorithm had very limited success in identifying the boundaries of the extremely faint aerosol layer in the free troposphere below 5 km. However, for those few identifications that were made, all features were classified as aerosol by both the GLAS algorithm and the CALIPSO algorithm.

[27] Because of the chaotic and occasionally ambiguous nature of the backscatter data below 2 km (especially from 2000:29 UTC on through the end of the acquisition sequence), correct labeling of all of the features in this region is a challenging task. As a consequence, making a quantitative assessment and comparison of classification success rates for the layers lying below 2 km is difficult. However, it still can be seen that most PBL aerosols and cloud-like layers were correctly discriminated by both the GLAS and CALIPSO algorithms. Differences between the two classification results are seen predominately at the edges of those cloud-like layers. Of the features within this ambiguous group, more were classified as aerosol by the GLAS algorithm than by the CALIPSO algorithm. A success rate of ~98.5% has been achieved by the CALIPSO algorithm for the features above 2 km in this case under study. The overall success rate for all altitudes is estimated to be better than 94%.

[28] Figures 6a and 6b present PDFs of volume color ratio and mean attenuated backscatter, respectively, derived by the GLAS and CALIPSO algorithms from the entire 10-flight data set for all altitudes. The PDFs derived by the two algorithms are generally consistent. However, several notable differences exist. In Figure 6a, relatively large differences are seen for volume color ratios larger than ~0.7. This is mostly due to the misclassification of cloud by the GLAS algorithm as demonstrated in Figure 5. This can be seen more clearly in Figures 7a and 7b, in which PDFs of volume color ratio and mean attenuated backscatter for 1–2-km altitudes are presented. A strong secondary mode appears at around 0.9 in the PDF of aerosol volume color ratio derived by GLAS. This mode is very similar to the mode of the corresponding cloud distribution, implying that contributions to the aerosol PDF in this high-color-ratio region are actually due to the misclassification of clouds as aerosols. This observation is consistent with our case studies and the results shown in Figure 5.

[29] The total feature occurrence number and the number of features that have been classified as different types by the GLAS and CALIPSO algorithm are plotted in Figure 8a as a function of feature center altitude. Two peaks in the difference curve are seen at 0–2-km and 5–8-km altitude regions. Figure 8b presents the ratio of the number of features classified as different types to the total feature number and the ratio of the number of features that have been classified as aerosol by GLAS and as cloud by CALIPSO to the total feature number. Among the features classified as different types, ~79% are those that have been classified as aerosol by GLAS and as cloud by CALIPSO. Most of these are clouds that have been classified as aerosol by GLAS as demonstrated in Figure 5. Above 8 km we ascribe the differences as being generally due to the incorrect classification of optically thin clouds as aerosols by the CALIPSO algorithm and to false positives such as those indicated in Figure 5b. Minor differences seen in Figure 6a for smaller color ratios are largely due to these high features. Here we note again that the prototype GLAS algorithm classifies all features above 8 km as cloud, resulting in a systematic misclassification of high-altitude aerosols (though we note, too, that only a small amount of aerosols were observed above 8 km by CPL during the THORPEX campaign).

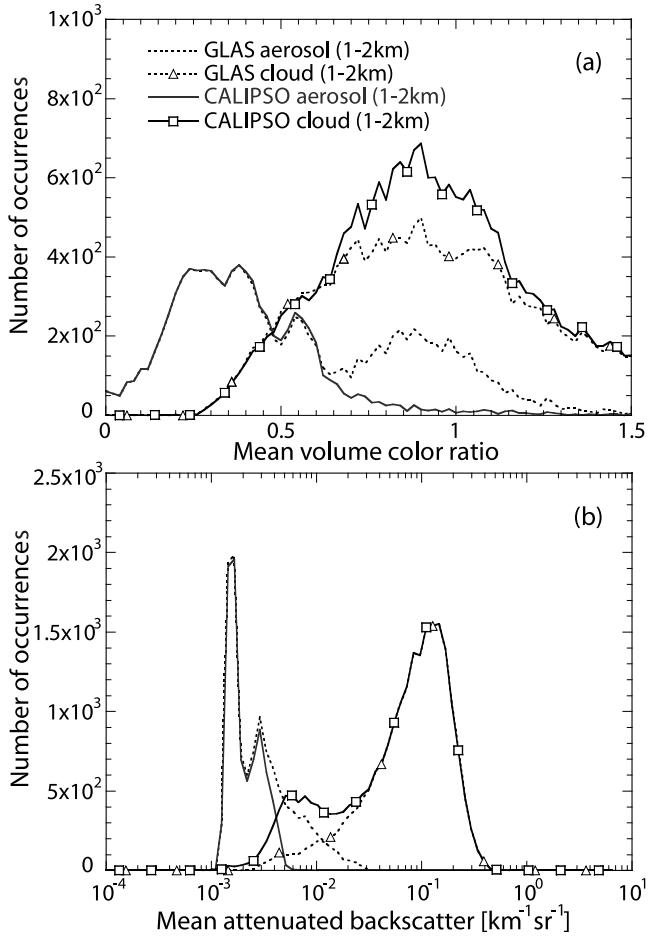

Figure 7. Distributions of (a) volume color ratio and (b) mean attenuated backscatter for 1–2-km altitudes.

[30] The results presented thus far show that the ability to discriminate between clouds and aerosols is improved by the multitest algorithm devised for CALIPSO. As mentioned in section 2.3, in a higher-dimensional space the

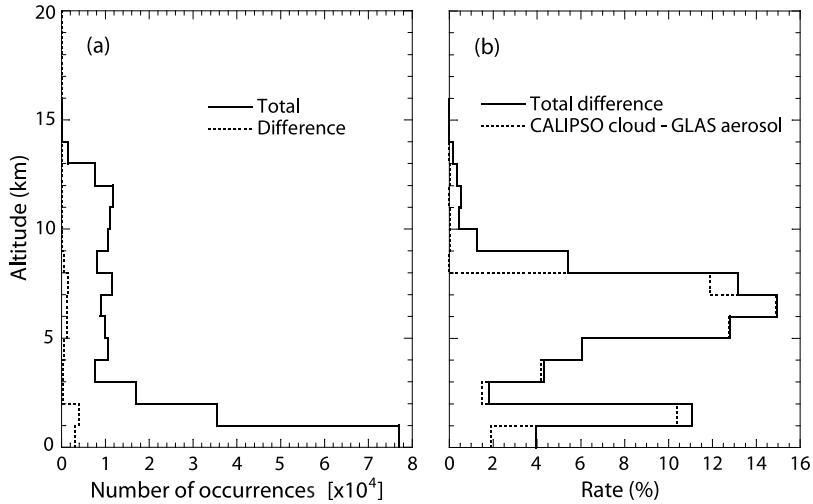

Figure 8. (a) Total occurrence number (solid line) of features and the number of features that were classified as different types by the GLAS and CALIPSO algorithms (dotted line). (b) Total difference rate (solid line) and difference rate of features classified as aerosol by GLAS and cloud by CALIPSO (dotted line).

different feature clusters separate more readily and distinctively than in lower dimensional space. The CALIPSO algorithm employs a 3-D approach (β'-χ'-z space). On the other hand, the GLAS discriminator is equivalent to a 2-D approach consisting of $p = \beta'_{max} \times |(\Delta\beta'/\Delta z)|_{max}$ and z. In this study, a better separation of cloud and aerosol clusters is achieved in the 3-D space. Figures 9a and 9b present scatterplots of mean volume color ratio and mean 532-nm attenuated backscatter, respectively, for the CALIPSO classified features. Clouds and aerosols are shown to separate well in the volume color ratio plot above ~1.5 km. Incorporating the volume color ratio into the classification scheme clearly contributes to the improved discrimination capability of the CALIPSO algorithm. However, some overlap still exists below ~1.5 km. Not surprisingly, incorrect classifications produced by the CALIPSO algorithm originate mostly in this altitude regime.

[31] We note that the cloud-aerosol classification with the two-dimensional GLAS algorithm may be improved somewhat by optimizing the selection of threshold values. However, the classification performance is limited intrinsically by the degree of the separation of cloud and aerosol clusters in the p-z space.

[32] It is also seen that volume color ratio decreases with altitude. As described in section 3.1, the volume color ratio is the ratio of total signals including particulate and molecular scattering. Its value varies between molecular color ratio and particulate color ratio depending on scattering ratio (the ratio of particulate backscattering coefficient to molecular backscattering coefficient). The 1064-nm to 532-nm molecular color ratio is 1/16 and is in general much smaller than the particulate color ratio. When the scattering ratio is very large, the volume color ratio is very close to the particulate color ratio, and it is close to the molecular color

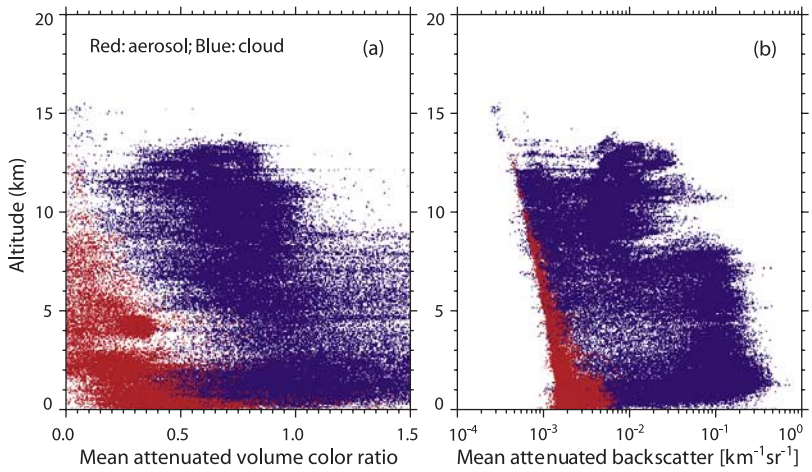

Figure 9. Scatterplots of mean attenuated (a) volume color ratio and (b) backscatter of the CALIPSO-algorithm-classified clouds and aerosols as a function of medium altitude of the feature layer for the CPL THORPEX data set.

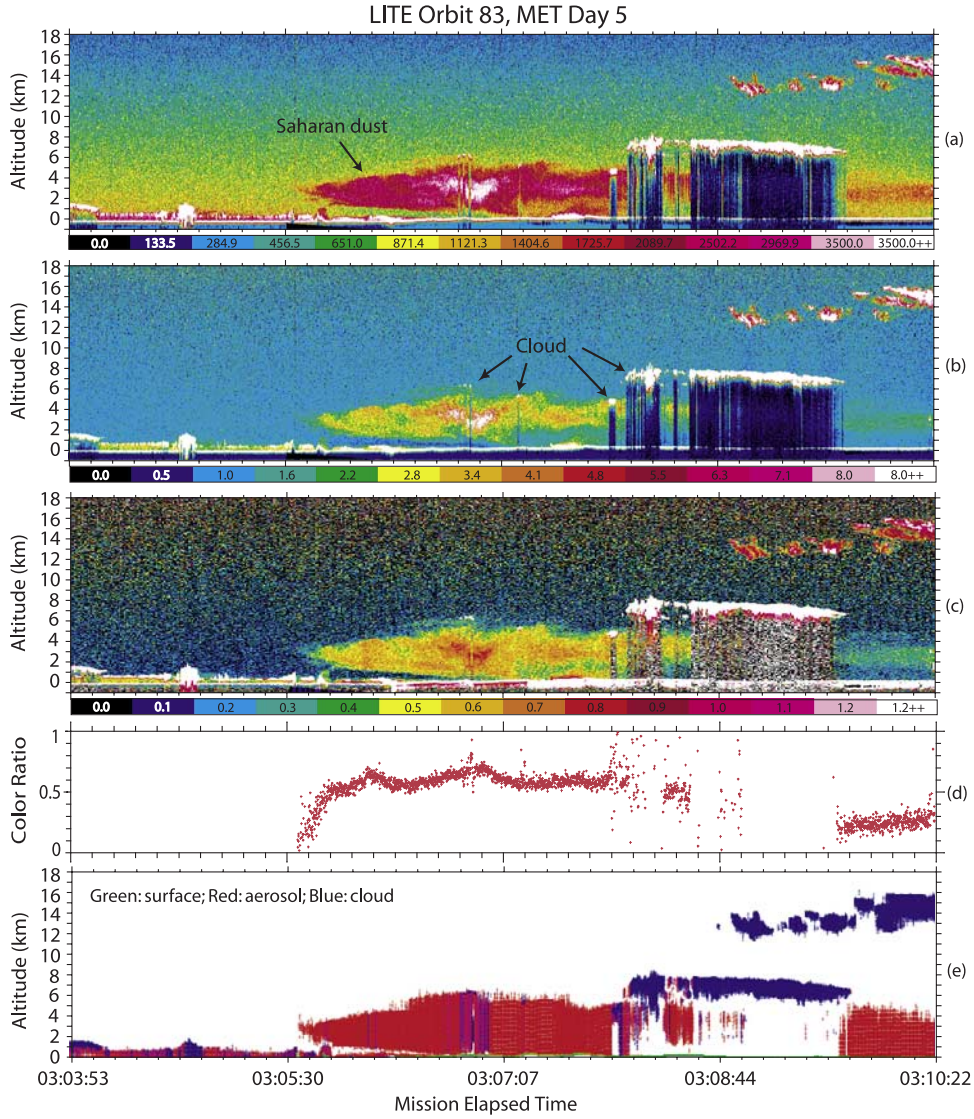

Figure 10. (a) Raw lidar signal at 532 nm, (b) attenuated scattering ratio at 532 nm, (c) 1064-nm to 532-nm volume color ratio, (d) layer-averaged attenuated volume color ratio, and (e) feature layer mask with the color indicating feature types classified by the CALIPSO cloud and aerosol classification algorithm.

ratio when the scattering ratio is very small. For higher features the scattering ratio is generally smaller than that for lower features, and the volume color ratio tends to be smaller at higher altitudes.

4.2. Using LITE Desert Dust Data

[33] As predicted by theory (e.g., see Figure 3) and demonstrated by observations [e.g., *Vaughan*, 2003; *Sugimoto et al.*, 2002], because of the larger particle sizes present, desert dust usually has a higher particulate color ratio than other aerosol types. The value of the color ratio for desert dust is very close to that for clouds. This fact alone may cause some additional difficulty in distinguishing dust aerosol from clouds at or near desert regions. When combined with the higher backscatter coefficients frequently found in desert dusts (which, in turn, are due to the high probability of large injections of mineral particles to the atmosphere in the regions), the potential for ambiguity is magnified further. A test of the CALIPSO algorithm specifically targeting dust data observed over a desert region was therefore highly desirable. LITE acquired observations on numerous orbits passing over the Sahara desert [*Winker et al.*, 1996]. Because the LITE data provide lidar backscatter profiles at three wavelengths (355 nm, 532 nm, and 1064 nm), it is well suited for testing the CALIPSO cloud-aerosol discrimination scheme. Hence LITE desert dust data were used to test the CALIPSO algorithm. Layer boundaries in the LITE backscatter profiles were located using a threshold-based feature finder [*Vaughan et al.*, 2002] applied to the 532-nm signal profiles. As in the tests using CPL data, the mean attenuated backscatter at 532 nm and the 1064-nm to 532-nm attenuated volume color ratio, along with the altitude midpoint of the layer, are used as input to the algorithm.

[34] Figure 10 presents an example of the LITE test data. Figure 10a shows a segment of 532-nm raw backscatter data acquired during orbit 83, as LITE passed over the western portion of the Sahara desert. The 532-nm attenuated

scattering ratio (that is, the ratio of the attenuated backscatter coefficients to a reference molecular profile) and the volume attenuated color ratio ($\beta'_{1064}(z)/\beta'_{532}(z)$ are plotted in Figures 10b and 10c, respectively. A layer of Saharan dust is seen from ~0305:30 mission elapsed time (MET) to the end of this data segment.

[35] This dust layer is geometrically thick, extending from the surface up to an altitude of 6 km at its thickest point. The attenuated scattering ratio is generally larger than 2.2 and, as seen in Figure 10b, increases to approximately 5 in the densest regions. Note, however, that the true maximum value of the attenuated scattering ratio cannot be ascertained because of signal saturation. As a consequence of the high gain settings used during this phase of the LITE mission, the 532-nm signal in this data segment saturates in clouds and in dense aerosols. In Figure 10a the saturated regions of the signal (e.g., the dense cloud at ~7 km, extending from 0308:05 to 0309:42 MET) are indicated in white. Mild signal saturation is seen in the denser parts of the dust layer and the PBL aerosol layer, but deep saturation is seen only in strong clouds. Though not presented here, no saturation of the 1064-nm signal occurred in the dust layer. As a result of this differential saturation, the color ratio was overestimated significantly in dense clouds and to a lesser degree in the denser parts of the dust and PBL aerosol layers.

[36] The values of attenuated scattering ratio for the dust layer are very similar to the range of 2–5 that was typically observed by a ground lidar for relatively calm weather conditions at Dunhuang (40°00′N, 94°30′W), an observation station that is very close to the Taklamakan Desert [*Iwasaka et al.*, 2003]. A range of peak scattering ratio of 1.4–5.2 was measured by a high-spectral-resolution-lidar (HSRL) at Tsukuba in Japan for a number of heavy Asian dust events during the springs of 1998 and 1999 [*Liu et al.*, 2002a]. The dust layers in these events are the result of transport eastward from the Asian desert regions in China and/or Mongolia following the very severe dust storms. The range of layer-averaged scattering ratios for these Asian dust events was from 1.3 to 3.4.

[37] The Saharan dust layer measured by LITE also has a large color ratio. An analysis by *Vaughan* [2003] estimates the particulate color ratio at ~0.86 for this layer. The mean attenuated volume color ratio for each profile, which was computed from the ratio of layer-averaged backscatters at 1064 nm and 532 nm, is presented in Figure 10d. Features' upper and lower boundaries were determined by a feature-finder algorithm [*Vaughan et al.*, 2002]. It can be seen that for the most part the volume color ratio is smaller than the particulate color ratio (~0.86) because of the presence of molecular scattering and (possibly) the spectral dependence of the attenuation. Large values are seen mainly in the denser parts of the dust layer. Large aerosol color ratios can also be measured when there are dense clouds overlying the dust layer. Because of attenuation from the clouds the return signal from the dust layer underneath is weakened at both 1064 nm and 532 nm, and the signal-to-noise ratio is likewise reduced substantially in both channels. In this situation, large color ratio values can occur as a result of noise excursions.

[38] The CALIPSO algorithm was applied to all features detected in this data segment. Results are presented in Figure 10e. As with the results obtained using the CPL data, the color used indicates the different feature types: Red represents aerosol, and blue represents cloud. The additional green color in Figure 10e denotes the surface. It is seen that for the most part the dust layer has been classified as aerosol. Approximately 8% of the dust layer has been misclassified as cloud. Within this 8%, the layer mean attenuated color ratio is typically in excess of ~0.7. The results shown in Figure 10e clearly demonstrate that the CALIPSO algorithm can effectively discriminate between dust layers and clouds even in the demanding conditions imposed by measurements acquired in desert regions. We have also tested with other dust data sets acquired during other CPL missions (e.g., Cirrus Regional Study of Tropical Anvils and Cirrus Layers–Florida Area Cirrus Experiment (CRYSTAL-FACE)). The dust layers contained in these data sets are generally less robust than the one shown in Figure 10. In these additional tests, better classification between dust layers and clouds was achieved.

4.3. Future Refinements

[39] In strong storm disturbances, dust aerosols at or near desert regions can have even larger backscatter coefficients and higher volume color ratio (approaching the dust particulate value) than those tested in this study. A very heavy dust event with a maximum extinction coefficient of ~4 km^{-1} has been recorded at a site (116.3°E, 39.9°N) in Beijing in 2002 by *Sugimoto et al.* [2003]. In such extreme conditions the likelihood that the CALIPSO algorithm will mistakenly classify a dust layer as a cloud is no doubt higher than would be indicated by the figures and numbers presented thus far.

[40] Therefore, in order to further refine and improve our ability to discriminate dust from clouds, we plan to conduct further testing using measurements made in desert regions. In addition, consideration will be given to extending the dimensionality of the PDFs used by including several supplementary optical and/or physical parameters. The physical thickness of a layer is one such example. Optically thick dust aerosol layers usually exist in the lower atmosphere and have a vertical extent of several kilometers. On the other hand, optically thick clouds in the lower atmosphere generally exhibit a much smaller physical thickness. Therefore, by including this additional dimension specifying the physical thickness of a feature, a better separation between the class of aerosols (including dust) and the class of clouds might be achieved.

[41] Another test, one that checks whether a feature layer is adjacent to the surface, can also be conducted to help separate clouds and aerosols in the PBL. The PBL aerosol layer is usually in contact with the surface, whereas cloud layers, except for some hazes and/or fogs, are not. The surface adjacency test might be implemented as follows. For features in the lower atmosphere, if confidence level computed using the multidimensional PDFs fails to exceed some threshold, then the layer would be checked to see whether it is adjacent to the surface. If the layer is found to be adjacent to the surface, then the layer is classified as aerosol. If not, then the initial (albeit low-confidence) classification made by the PDF approach is retained. As seen in Figure 9, there is more overlap between the cloud and aerosol clusters in the PBL than at other altitudes. Similarly, misclassification of the THORPEX-PTOST data by the CALIPSO algorithm

occurs mainly in the PBL region. It would seem therefore that additional testing of features found in this altitude regime would be warranted.

[42] The volume depolarization ratio is a useful indicator for identifying irregular particles [e.g., *Sassen*, 1991; *Murayama et al.*, 2001; *Liu et al.*, 2002a], and it provides the means to discriminate between ice clouds and water clouds and between dust layers and spherical aerosols. This parameter is also a candidate for inclusion in the parameter space used for cloud-aerosol discrimination. At lower altitudes the depolarization ratio should be especially helpful in distinguishing dense desert dust aerosols from water clouds. Nonspherical dust particles can produce high depolarization ratios [*Gobbi et al.*, 2000; *Murayama et al.*, 2001], whereas when multiple scattering can be neglected, the spherical droplets in water clouds generally yield no depolarization. However, we note here that for spaceborne lidars the depolarization due to the multiple scattering in dense water clouds could be an issue [*Hu et al.*, 2001]: The high altitude of the orbit (e.g., 705 km for the CALIPSO satellite) can yield a large footprint on the ground even for a small receiver field of view. Introducing a depolarization ratio test into the CALIPSO algorithm would thus require the development of PDFs for cloud and aerosol depolarization ratios that correctly account for the effects of multiple scattering. Unfortunately, as neither LITE nor GLAS was configured as a polarization-sensitive instrument, no space-based measurements of depolarization ratio are available for testing such PDFs. Therefore it is currently difficult to make reliable assessments regarding the utility of an additional depolarization ratio test. However, revisiting the issue will become possible once sufficient data have been collected by the CALIPSO mission itself.

5. Conclusions

[43] Single-test and multiple-test approaches based on 1-D or multiple-D PDFs for the two-class scene classification problem have been studied and described in this paper. We have shown that the multiple-test approach provides better classification than a single-test approach. Theoretically, a better classification can be achieved by adding more tests, because the separation of different feature clusters, which is a basic limitation of the classification, is more complete in higher-dimensional space. A practical algorithm has been developed for the CALIPSO lidar cloud-aerosol discrimination. The algorithm is a 3-D approach utilizing the layer mean attenuated backscatter at 532 nm, the layer-integrated 1064-nm to 532-nm volume color ratio, and the midlayer altitude.

[44] The algorithm has been tested with the data set of 49 hours acquired by CPL during the 2003 THORPEX-PTOST campaign conducted in Honolulu, Hawaii, from 18 February to 14 March 2003. All 228,264 features found in this data set were used as input to the algorithm test. Feature classifications generated by the CALIPSO algorithm were compared to those generated by the GLAS prototype algorithm and included in the CPL data product. The majority of features were classified identically by the two algorithms. However, in ~5.7% of the cases the algorithms arrived at different conclusions. Case studies revealed that these differences are mostly due to the misclassification of cloud as aerosol by the GLAS algorithm. The introduction of volume color ratio as a test criterion in the CALIPSO algorithm has significantly improved the cloud-aerosol classification, because better separation of cloud and aerosol clusters can be achieved.

[45] Because their scattering properties (especially color ratio) are so similar to clouds, dust aerosols are judged to present the highest potential for misclassification by the CALIPSO algorithm. For this reason, additional tests of the CALIPSO algorithm were conducted using LITE dust data acquired over the Sahara desert. For those dust events observed far from the desert region, features are correctly identified as being either cloud or (dust) aerosol. For the dust event measured during LITE orbit 83, dust identification was in general quite successful. However, several instances in which the layer-integrated attenuated color ratio was larger than ~0.7 were incorrectly classified as cloud. In these cases, the large color ratio values were either caused by noise or due to the contamination of the dust layer by embedded or vertically adjacent clouds. Saturation in the return signals also resulted in occasional overestimation of the color ratio in the dust layer. Additional tests on layer thickness and/or on whether the layer is in contact with the surface are proposed as future improvements to help to discriminate aerosols in the PBL. Another proposed modification is the inclusion of volume depolarization ratio in the parameter space used for cloud-aerosol discriminations. The algorithm is being implemented for the launch of CALIPSO in early 2005.

References

Bevington, P. R., and D. K. Robinson (1992), *Data Reduction and Error Analysis for the Physical Sciences*, McGraw-Hill, New York.

Beyerle, G., et al. (2001), A lidar and backscatter sonde measurement campaign at Table Mountain during February–March 1997: Observations of cirrus clouds, *J. Atmos. Sci.*, *58*, 1275–1287.

Bösenberg, J., et al. (2003), EARLINET: A European Aerosol Research Lidar Network to establish an aerosol climatology, *MPI-Rep. 348*, Max-Planck-Inst. für Meteorol., Hamburg, Germany.

Gobbi, G. P., F. Barnaba, R. Giorgi, and A. Santacasa (2000), Altitude-resolved properties of a Saharan dust event over the Mediterranean, *Atmos. Environ.*, *34*, 5119–5127.

Hess, M., R. Koelemeijer, and P. Stammes (1998a), Scattering matrices of imperfect hexagonal ice crystals, *J. Quant. Spectrosc. Radiat. Transfer*, *60*, 301–308.

Hess, M., P. Koepke, and I. Schult (1998b), Optical properties of aerosols and clouds: The software package OPAC, *Bull. Am. Meteorol. Soc.*, *79*, 831–844.

Hu, Y., D. Winker, P. Yang, B. Baum, L. Poole, and L. Vann (2001), Identification of cloud phase from PICASSO-CENA lidar depolarization: A multiple scattering sensitivity study, *J. Quant. Spectrosc. Radiat. Transfer*, *70*, 569–579.

Iwasaka, Y., et al. (2003), Large depolarization ratio of free tropospheric aerosols over the Taklamakan Desert revealed by lidar measurements: Possible diffusion and transport of dust particles, *J. Geophys. Res.*, *108*(D23), 8652, doi:10.1029/2002JD003267.

Liu, Z., and N. Sugimoto (2002), Simulation study for cloud detection with space lidars by use of analog detection photomultiplier tubes, *Appl. Opt.*, *41*, 1750–1759.

Liu, Z., P. Voelger, and N. Sugimoto (2000), Simulations of the observation of clouds and aerosols with the Experimental Lidar in Space Equipment system, *Appl. Opt.*, *39*, 3120–3137.

Liu, Z., N. Sugimoto, and T. Murayama (2002a), Extinction-to-backscatter ratio of Asian dust observed with high-spectral-resolution lidar and Raman lidar, *Appl. Opt.*, *41*, 2760–2767.

Liu, Z., M. A. Vaughan, L. R. Poole, C. A. Hostetler, and D. M. Winker (2002b), Scene classification for the CALIPSO lidar, paper presented at 21st International Laser Radar Conference, Opt. Soc. of Am., Quebec City, Que., Canada.

Matthias, V., and J. Bösenberg (2002), Aerosol climatology for the planetary layer derived from regular lidar measurements, *Atmos. Res.*, *63*, 221–245.

McGill, M. J., D. L. Hlavka, W. D. Hart, J. D. Spinhirne, V. S. Scott, and B. Schmid (2002), The cloud physics lidar: Instrument description and initial measurement results, *Appl. Opt.*, *41*, 3725–3734.

McIntyre, R. J. (1972), The distribution of gains in uniformly multiplying avalanche photodiode: Theory, *IEEE Trans. Electron Devices*, *ED-19*, 703–713.

Murayama, T., et al. (2001), Ground-based network observation of Asian dust events of April 1998 in east Asia, *J. Geophys. Res.*, *106*, 18,345–18,359.

Omar, A., J. Won, S. Yoon, and M. P. McCormick (2002), Estimation of aerosol extinction-to-backscatter ratios using AERONET measurements and cluster analysis, paper presented at 21st International Laser Radar Conference, Opt. Soc. of Am., Quebec City, Que., Canada.

Palm, S., W. Hart, D. Hlavka, E. Welton, A. Mahesh, and J. Spinhirne (2002), Geoscience Laser Altimeter System (GLAS) Algorithm Theoretical Basis Document Version 4.2: GLAS atmospheric data products, NASA Goddard Space Flight Cent., Greenbelt, Md., Oct.

Platt, C. M. R., S. A. Young, P. J. Manson, G. R. Patterson, S. C. Marsden, R. T. Austin, and J. H. Churnside (1998), The optical properties of equatorial cirrus from observations in the ARM Pilot Radiation Observation Experiment, *J. Atmos. Sci.*, *55*, 1977–1996.

Reagan, M. J., X. Wang, and M. J. Osborn (2002), Spaceborne lidar calibration from cirrus and molecular backscatter returns, *IEEE Trans. Geosci. Remote Sens.*, *40*, 2285–2290.

Sasano, Y., and E. V. Browell (1989), Light scattering characteristics of various aerosol types derived from multiple wavelength lidar observations, *Appl. Opt.*, *28*, 1670–1679.

Sassen, K. (1991), The polarization lidar technique for cloud research: A review and current assessment, *Bull. Am. Meteorol. Soc.*, *72*, 1848–1866.

Sugimoto, N., I. Matsui, A. Shimizu, I. Uno, K. Asai, T. Endoh, and T. Nakajima (2002), Observation of dust and anthropogenic aerosol plumes in the Northwest Pacific with a two-wavelength polarization lidar on board the research vessel *Mirai*, *Geophys. Res. Lett.*, *29*(19), 1901, doi:10.1029/2002GL015112.

Sugimoto, N., I. Uno, M. Nishikawa, A. Shimizu, I. Matsui, X. Dong, Y. Chen, and H. Quan (2003), Record heavy Asian dust in Beijing in 2002: Observations and model analysis of recent events, *Geophys. Res. Lett.*, *30*(12), 1640, doi:10.1029/2002GL016349.

Vaughan, M. A. (2003), Algorithm for retrieving lidar ratios at 1064 nm from space-based lidar backscatter data, in *Laser Radar Technology for Remote Sensing*, edited by C. Werner, *Proc. SPIE Int. Soc. Opt. Eng.*, *5240*, 104–115.

Vaughan, M. A., D. M. Winker, and C. A. Hostetler (2002), SIBYL: A selective iterated boundary location algorithm for finding cloud and aerosol layers in CALIPSO lidar data, paper presented at 21st International Laser Radar Conference, Opt. Soc. of Am., Quebec City, Que., Canada.

Wang, Z., and K. Sassen (2001), Cloud type and macrophysical property retrieval using multiple remote sensors, *J. Appl. Meteorol.*, *40*, 1665–1682.

Winker, M., R. Couch, and M. P. McCormick (1996), An overview of LITE: NASA's Lidar In-space Technology Experiment, *Proc. IEEE*, *84*, 164–180.

Winker, D. M., J. R. Pelon, and M. P. McCormick (2003), The CALIPSO mission: Spaceborne lidar for observation of aerosols and clouds, *Proc. SPIE Int. Soc. Opt. Eng.*, *4893*, 1–11.

Young, S. A. (1995), Analysis of lidar backscatter profiles in optically thin clouds, *Appl. Opt.*, *34*, 7019–7031.

W. Hart, D. Hlavka, and M. McGill, NASA Goddard Space Flight Center, Code 912, Greenbelt, MD 20771, USA. (billhart@virl.gsfc.nasa.gov; sgdlh@virl.gsfc.nasa.gov; mcgill@virl.gsfc.nasa.gov)

C. A. Hostetler, L. R. Poole, M. A. Vaughan, and D. M. Winker, NASA Langley Research Center, Mail Stop 435, Hampton, VA 23681, USA. (c.a.hostetler@larc.nasa.gov; l.r.poole@larc.nasa.gov; ma.vaughan@larc.nasa.gov; d.m.winker@larc.nasa.gov)

Z. Liu, Center for Atmospheric Sciences, Hampton University, 23 Tyler Street, Hampton, VA 23668, USA. (z.liu@larc.nasa.gov)